Intestinal invalidation of the glucose transporter GLUT2 delays tissue distribution of glucose and reveals an unexpected role in gut homeostasis

Charlotte C. Schmitt, Thomas Aranias, Thomas Viel, Danielle Chateau, Maude Le Gall, Anne-Judith Waligora-Dupriet, Chloé Melchior, Ophélie Rouxel, Nathalie Kapel, Guillaume Gourcerol, et al.

HAL Id: hal-01501611

https://hal.sorbonne-universite.fr/hal-01501611

Submitted on 4 Apr 2017

Intestinal invalidation of the glucose transporter GLUT2 delays tissue distribution of glucose and reveals an unexpected role in gut homeostasis

Charlotte C. Schmitt [1], Thomas Aranias [1], Thomas Viel [2], Danielle Chateau [1], Maude Le Gall [1,8], Anne-Judith Waligora-Dupriet [3], Chloé Melchior [4], Ophélie Rouxel [5], Nathalie Kapel [6], Guillaume Gourcerol [4], Bertrand Tavitian [2], Agnès Lehuen [5], Edith Brot-Laroche [1], Armelle Leturque [1], Patricia Serradas [1], Alexandra Grosfeld [1,*]

ABSTRACT

Objective: Intestinal glucose absorption is orchestrated by specialized glucose transporters such as SGLT1 and GLUT2. However, the role of GLUT2 in the regulation of glucose absorption remains to be fully elucidated.

Methods: We wanted to evaluate the role of GLUT2 on glucose absorption and glucose homeostasis after intestinal-specific deletion of GLUT2 in mice (GLUT2$^{\Delta IEC}$ mice).

Results: As anticipated, intestinal GLUT2 deletion provoked glucose malabsorption as visualized by the delay in the distribution of oral sugar in tissues. Consequences of intestinal GLUT2 deletion in GLUT2$^{\Delta IEC}$ mice were limiting body weight gain despite normal food intake, improving glucose tolerance, and increasing ketone body production. These features were reminiscent of calorie restriction. Other adaptations to intestinal GLUT2 deletion were reduced microvillus length and altered gut microbiota composition, which was associated with improved inflammatory status. Moreover, a reduced density of glucagon-like peptide-1 (GLP-1) positive cells was compensated by increased GLP-1 content per L-cell, suggesting a preserved enteroendocrine function in GLUT2$^{\Delta IEC}$ mice.

Conclusions: Intestinal GLUT2 modulates glucose absorption and constitutes a control step for the distribution of dietary sugar to tissues. Consequently, metabolic and gut homeostasis are improved in the absence of functional GLUT2 in the intestine, thus mimicking calorie restriction.

1. INTRODUCTION

The intestine responds to the external environment by complex interplays between cells in the epithelium, the immune system, and microbes. Gut homeostasis allows a permanent adaptation to nutritional, metabolic, or bacterial signals through continuous renewal and differentiation of epithelial cells. After carbohydrate intake and digestion, sugars are absorbed in the proximal small intestine by several specialized transporters. The Na$^+$/glucose cotransporter SGLT1 triggers glucose absorption at the food-facing membrane. GLUT2 facilitates the passage of dietary sugars, glucose, fructose, and galactose towards the bloodstream [1]. In enterocytes, GLUT2 is consistently located in the basolateral membrane but, during a sugar rich meal, can be recruited transiently to the apical membrane, where it remains permanently in case of insulin resistance [2–4]. GLUT2 is expressed in enteroendocrine cells, especially in L-cells [5]. L-cells express nutrient transporters and receptors that can sense luminal nutrients at their apical membrane and thereby influence their own functions [6,7]. Enteroendocrine cells are scattered in the intestinal epithelium and constitute the largest population of hormone-producing

[1] INSERM UMR-S 1138, Centre de Recherche des Cordeliers, Sorbonne Universités, UPMC Univ Paris 06, Sorbonne Cités, UPD Univ Paris 05, CNRS, IHU ICAN, Paris, France [2] Plateforme imagerie du vivant, Centre de Recherche Cardiovasculaire de Paris, INSERM U970, Université Paris Descartes-Sorbonne Paris cité, Paris, France [3] EA4065, Faculté de pharmacie, Université Paris Descartes, Sorbonne Paris Cité, 75006 Paris, France [4] INSERM UMR-1073, Gastroenterology Department, Rouen University Hospital, Rouen, France [5] INSERM U1016 and CNRS UMR8104, Institut Cochin, Laboratoire d'Excellence INFLAMEX, Paris, France [6] Service de Coprologie Fonctionnelle, Hopital La Pitié Salpêtrière, Paris, France

[8] Present address: INSERM UMRS 1149, Université Paris Diderot, Sorbonne Paris Cite, DHU Unity APHP, Paris, France.

*Corresponding author. Fax: +33 143251615. E-mail: alexandra.grosfeld@crc.jussieu.fr (A. Grosfeld).

Abbreviations: 2FDG, 2-deoxy-2-[^{18}F]fluoro-D-glucose; DPP-IV, dipeptidyl-peptidase IV; GLP-1, glucagon-like peptide-1; GLUT1-7, glucose transporter 1–7; IEC, intestinal epithelial cells; IL, interleukin; IPGTT, intraperitoneal glucose tolerance test; ITT, insulin tolerance test; OGTT, oral glucose tolerance test; PET-CT, Positron Emission Tomography-Computed Tomography; SGLT1, sodium-glucose transporter 1

Received October 17, 2016 • Revision received October 20, 2016 • Accepted October 26, 2016 • Available online 4 November 2016

http://dx.doi.org/10.1016/j.molmet.2016.10.008

cells of the body. L-cells produce incretins such as glucagon-like peptide-1 (GLP-1), a potent activator of glucose-induced insulin secretion [8]. It is now thought that sufficient L-cells are present in the proximal intestine to account for early rises of GLP-1 after a meal. However, when absorption is reduced, the higher nutrient delivery to distal intestine may bring more L-cells in contact with nutrients and/or their microbial fermentation products, resulting in increased plasma GLP-1 levels [9].

Physiological studies of genetically modified mice have revealed a role for GLUT2 in several regulatory mechanisms. A total knockout of GLUT2 in mouse indicated that GLUT2 is dispensable for intestinal glucose absorption because of the existence of compensatory mechanisms [10]. However, Glut2$^{-/-}$;RIPGlut1 mice rescued by GLUT1 expression in pancreatic β cells displayed impaired plasma GLP-1 levels after glucose gavage, which was attributed to reduced intestinal GLP-1 content [11], suggesting that GLUT2 is of importance in L-cell function. In the present study, our hypothesis was that intestinal GLUT2 could contribute to both metabolic and gut homeostasis. Impaired glucose absorption in the small intestine could cause disturbed glucose delivery, modified gut microbiota composition, and altered L-cell function. To test this hypothesis, we generated an inducible model of GLUT2 invalidation in intestinal epithelial cells.

2. MATERIAL AND METHODS

2.1. Generation of transgenic mice with targeted deletion of *Slc2a2* in the intestine

Heterozygous *Slc2a2*[tm1a(KOMP)Wtsi] mice were generated by the KnockOut Mouse Project (KOMP) at the University of California, Davis (Project ID#CSD40514), using the targeting vector described in Figure 1A(a). This vector contains the lacZ expressing cassette with polyA tail inserted between Exon 3 and Exon 4 of *Slc2a2*, generating a null allele that produces β-galactosidase in cells with active *Slc2a2* gene transcription (Figure 1A(a)). We could observe that heterozygous mice survived and expressed β-galactosidase in GLUT2 expressing tissues including the intestine (data not shown). These founder mice were crossed with mice that express the Flippase recombinase to remove the lacZ and neomycin cassettes generating *Slc2a2*[FLOX/FLOX] mice (Figure 1A(b)). *Slc2a2*[FLOX/FLOX] mice were then crossed with a *Villin-CreERT2* mouse line [12] (gift from S. Robine) to generate *Slc2a2*[FLOX/FLOX] × *Villin-CreERT2*^{+/−} and *Slc2a2*[FLOX/FLOX] × *Villin-CreERT2*^{−/−} mice. In the *Slc2a2*[FLOX/FLOX] × *Villin-CreERT2*^{+/−} mice, Cre recombinase was activated by tamoxifen gavage (1 mg/mouse; Sigma–Aldrich) for 3 consecutive days to induce a specific *Slc2a2* deletion in intestinal epithelial cells (GLUT2[ΔIEC] mice, Figure 1A(c)).
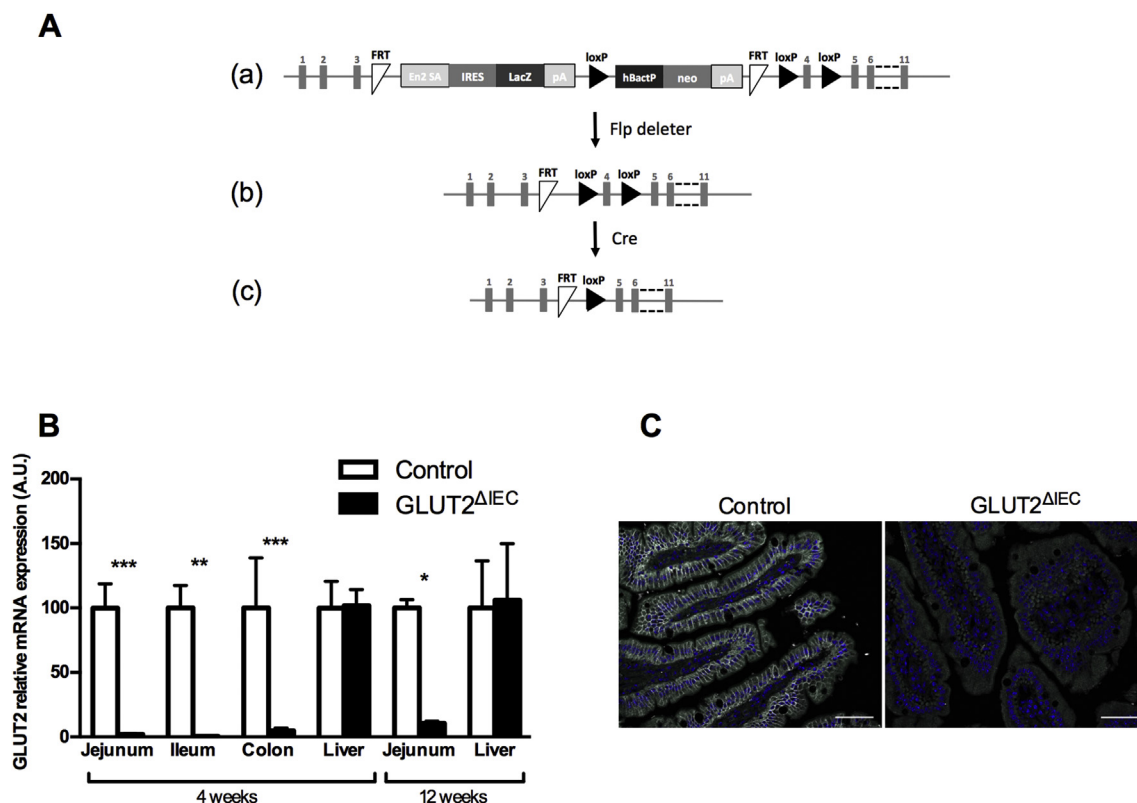

Figure 1: Generation of GLUT2[ΔIEC] mice. (A) (a) The *Slc2a2*/lacZ knock-in allele (*Slc2a2*(KOMP)Wtsi) is shown to illustrate the mutated *Slc2a2* gene, in which the lacZ and neomycin expression cassettes were inserted between Exon 3 and Exon 4 and which is flanked by FRT (Flippase Recognition Target) sites. This cassette contains the splice acceptor of mouse engrailed 2 exon 2 (En2 SA), an internal ribosome entry sequence (IRES) to initiate lacZ translation, and polyadenylation (pA) to terminate transcription after the lacZ gene. The neo gene is driven by human beta actin promoter (hBactP) and contains its own pA. Additionally, Exon 4 is flanked by loxP sites. (b) The resulting *Slc2a2* conditional knockout gene structure is shown to illustrate removal of the lacZ and neomycin cassettes; it is generated by crossing Slc2a2[tm1a(KOMP)Wtsi] mice with mice that express the Flp recombinase. (c) The resulting *Slc2a2* knockout allele generated after crossing with Cre expressing mice and activation by tamoxifen gavage is shown. (B) Relative mRNA levels of sugar transporter GLUT2 in the jejunum, ileum, colon, and liver 4 weeks after tamoxifen administration and in the jejunum and liver 12 weeks after tamoxifen administration in control (white bars, n = 4−8) and GLUT2[ΔIEC] (black bars, n = 3−9) mice. Values are means ± SEM. *P < 0.05, **P < 0.01, ***P < 0.001; control *vs* GLUT2[ΔIEC] mice (Mann–Whitney *U* test). (C) Jejunal sections from control (left panel) and GLUT2[ΔIEC] (right panel) mice 4 weeks after tamoxifen administration were immunostained for GLUT2 (white) and DAPI (blue). Scale bars = 50 μm. Note the absence of GLUT2 labeling in jejunum of GLUT2[ΔIEC] mice.

$Slc2a2^{FLOX/FLOX} \times Villin\text{-}CreERT2^{-/-}$ received the same tamoxifen gavage and were used as littermate controls (control mice). All mice were on a C57BL/6J background. Mice were housed in the Cordeliers research center animal facility (Paris, France) with a 12:12-h light–dark cycle and allowed access to standard chow diet (SAFE R03) and water *ad libitum*. Mice were genotyped using the following PCR primers: CreVillin F: 5′-CAAGCCTGGCTCGACGGCC-3′; R: 5′-CGCGAA-CATCTTCAGGTTCT-3′; Glut2Flox F: 5′-TCTTGGCTTTGGGTGAAAAT-GAGCA-3′; R2: 5′-GAACTTCGGTTCCGGCGCCA-3′ (floxed allele, 239 bp); R7: 5′-AGGAGCAGTGGTTTGGATGGCA-3′ (wild-type allele, 201 bp). All animal use followed the French ethical guidelines for animal studies and was approved by the Regional Animal Care and Use Committee (CREEA Ile de France No. 3, agreement number 05210.02).

Body weight measurements and oral glucose tolerance tests were performed weekly until the 12th week after tamoxifen administration. All other experiments were performed 4 and/or 12 weeks after tamoxifen administration.

2.2. Glucose and insulin tolerance tests

All experiments were performed on conscious mice. For oral glucose tolerance test (OGTT) or intraperitoneal glucose tolerance test (IPGTT), overnight fasted (16 h) mice received a glucose load (4 g/kg body weight) orally or intraperitoneally, respectively. For insulin tolerance test (ITT), mice fasted for 6 h were injected intraperitoneally with 1 U/kg insulin (Actrapid, Novo Nordisk). For both tests, blood glucose was measured at the tail vein with an AccuCheck Performa glucometer (Roche Diagnostics) at 0, 5, 10, 30, 60, and 120 min. Glucose absorption through the intestine was quantified by calculating the glycemic slope between 0 and 5 min after an oral glucose load.

2.3. Plasma hormones and metabolites

GLP-1 and insulin levels were measured immediately before and 30-min after 2 g/kg D-glucose and 100 μL olive oil challenge to mimic a meal in mice fasted overnight (16 h). Blood samples were collected from the tail vein in EDTA-precoated tubes containing DPP-IV inhibitor (DPP4-010, Millipore). Plasma active GLP-1 levels were determined using high sensitivity GLP-1 active chemiluminescent ELISA kit (EMD Millipore Corporation). Plasma insulin levels were measured using ultrasensitive insulin ELISA kit (Alpco). Plasma β-hydroxybutyrate was measured using an automatic chemistry analyzer AU400 (Olympus Diagnostics) in blood samples collected from non-fasted mice.

2.4. Imaging intestinal glucose absorption and biodistribution using 2FDG-PET-CT

Control and GLUT2$^{\Delta IEC}$ mice were fasted overnight and subjected to Positron Emission Tomography-Computed Tomography (PET-CT) using the radiotracer 2-deoxy-2-[^{18}F]fluoro-D-glucose (2FDG) to assess intestinal glucose absorption and biodistribution in peripheral tissues. Mice were anesthetized with 1–2% isoflurane (IsoVet 100%, Centravet) in 100% O$_2$ during the whole experiment. PET acquisitions were acquired in the PET-CT scanner (nanoScan PET-CT, Mediso) 1 min after oral gavage of 10 MBq 2FDG (Gluscan, Advanced Applied Applications) in a saline solution containing 4 g/kg of D-glucose. Body temperature and respiration were registered. List-mode PET data were collected between 1 and 60 min post-injection, binned using a 5-ns time window, a 400- to 600-keV energy window, and a 1:5 coincidence mode. At the end of the PET acquisitions, CT scans were performed using the following parameters: mode semi-circular, tension of 39 kV, 720 projection full scan, 300 ms per projection, binning 1:4. After the *in vivo* scans, mice were sacrificed and the whole intestine was isolated and flushed to remove intraluminal 2FDG for *ex vivo* PET-

CT acquisition of 5 min. *In vivo* PET acquisitions were reconstructed in 12 frames of 5 min using the Tera-Tomo reconstruction engine (3D-OSEM based manufactured customized algorithm) with expectation maximization iterations, scatter, and attenuation correction. Images were analyzed using the software PMOD (PMOD Technologies LLC). Standardized Volume of Interest (VOI) was drawn in each organ, and Standardized Uptake Values (SUV) were calculated by dividing the mean tissue radioactivity concentration by the total orally administrated 2FDG and body weight.

2.5. Intestinal transit time

Carmine red was given by gavage to mice fasted for 6 h (10 mg/mL of water, 10 μL/g body weight). The total intestinal transit time was measured by determination of time between ingestion of carmine red and first appearance of the dye in feces.

2.6. Jejunal permeability

Jejunal permeability was assessed by measuring FITC-dextan (4 kDa, FD4) fluxes in Ussing chambers with an exchange surface of 0.07 cm^2 (Harvard Apparatus). FD4 (5 mg/mL) was placed at the mucosal side. After 3 h at 37 °C, medium from the serosal side was removed and stored at −80 °C. The fluorescence level of FD4 in serosal side (excitation at 485 nm, emission at 535 nm) was measured in 96-well black plate with spectrometer Chameleon V (Hidex). Values were converted to concentration using a standard curve.

2.7. Metabolic and stool analysis

Control and GLUT2$^{\Delta IEC}$ mice were housed individually in metabolic cages (Techniplast), 3 weeks after tamoxifen administration. After a 5- to 7-day adaptation period with *ad libitum* access to water and powdered chow diet, experiments were performed for a period of 7 days. Body weight, food and water intakes, and urine and fecal outputs were recorded daily. Stools were collected daily and stored at −20 °C. Stools collected for 2 days were pooled and analysed on homogenized samples. Total energy content was determined by calorimetry (PARR 1351 Bomb Calorimeter, Parr Instrument Company). 24-hour fecal calorie loss represented the proportion of ingested energy recovered in stool output.

2.8. Fecal microbiota analysis

Total DNA was extracted from frozen fecal samples using the chemical guanidine thiocyanate and the mechanical bead-beating method as described previously [13]. TaqMan® qPCR was used to quantify total bacterial population and the dominant (>1% of fecal bacterial population) bacterial groups, and genera: *Clostridium* cluster IV (*Clostridium leptum* group) and *Bacteroides*/*Prevotella* group. qPCR using SYBR-Green® was performed to quantify *Lactobacillus/Leuconostoc/Pediococcus* group, *Akkermansia muciniphila*, *Staphylococcus* and *Enterococcus* sp. (primers and probes reported in Supplementary Table 1). Standard curves were obtained from serial dilutions of a known concentration of plasmid DNA containing a 16S rRNA gene insert from each species or group. The coefficients of correlation between log10 CFU and rRNA gene copy numbers for each species and group were obtained from rrnDB (https://rrndb.umms.med.umich.edu/), which allowed the calculation of the number of CFU/g of feces. When species or targeted taxonomic groups were not detected, the arbitrary value of 1.5 log10 CFU/g of feces was used.

2.9. Glucose transporter and cytokine tissue expression analysis

Jejunal, ileal, colonic mucosa, and liver were collected, snap frozen, and kept at −80 °C until RNA extraction using RNeasy Mini kit
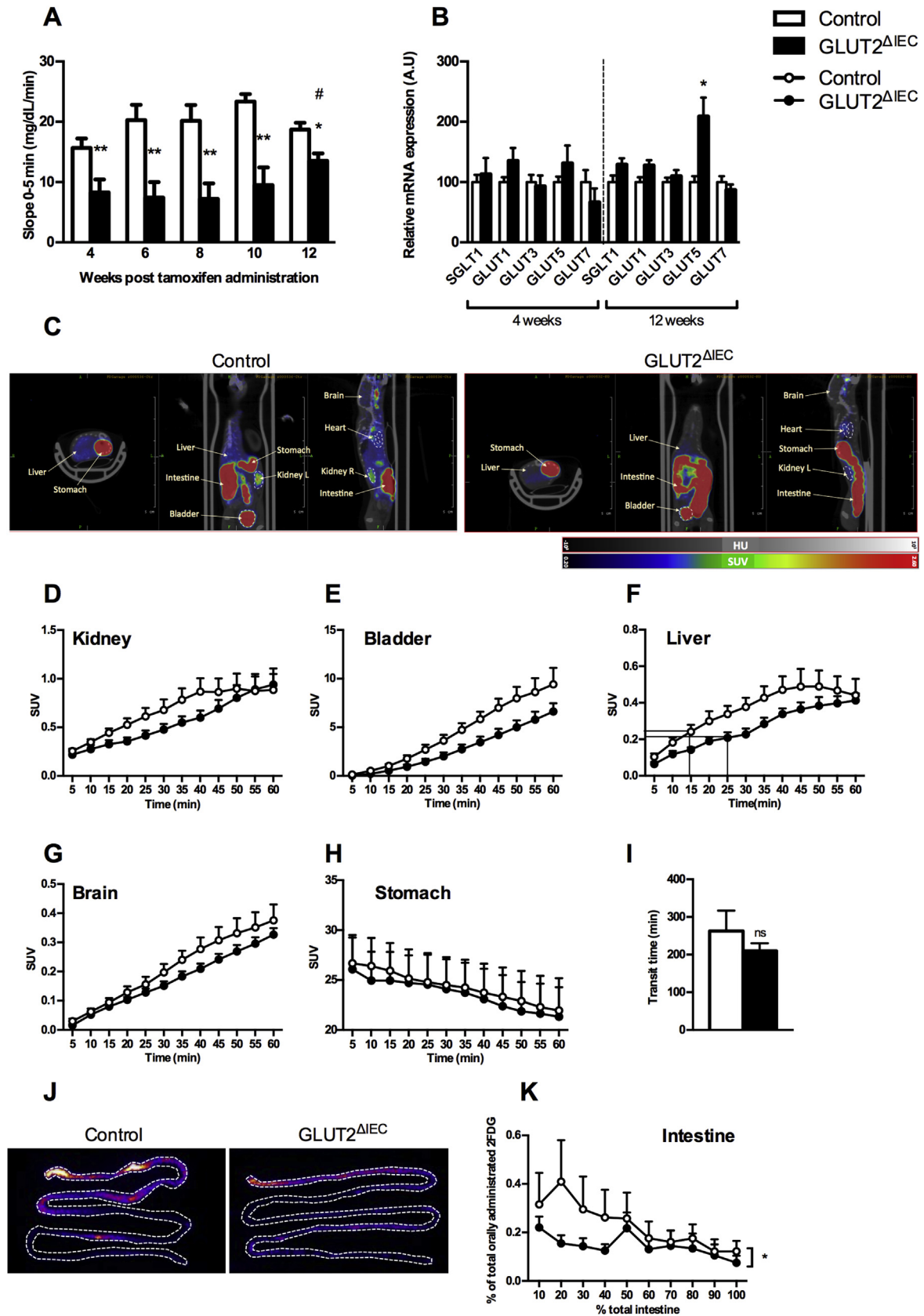
Figure 2: GLUT2^ΔIEC mice display glucose malabsorption. (A) Glucose absorption index was evaluated by the glycemic slopes calculated using blood glucose levels measured between 0 and 5 min after oral glucose bolus (4 g glucose/kg) in control (white bars, n = 10) and GLUT2^ΔIEC mice (black bars, n = 11), from 4 to 12 weeks after tamoxifen administration. Values are means ± SEM. *P < 0.05; **P < 0.01; Control *vs* GLUT2^ΔIEC (Mann−Whitney *U* tests). #P < 0.05; GLUT2^ΔIEC 4 *vs* 12 weeks post-tamoxifen

(Qiagen). For interleukin mRNA gene transcription assessment, ileal *lamina propria* lymphocytes were enriched using Lamina Propria dissociation kit (Miltenyi Biotech) prior to RNA extraction. One microgram of RNA was reverse transcribed with 200 units of reverse transcriptase using the Superscript II kit (Invitrogen) according to manufacturer's recommendations. RT-qPCR analysis was performed with a LightCycler 480 instrument (Roche Applied Science), and cDNA was amplified using SYBR® Green PCR Master Mix (Roche Applied Science) and specific primers reported in Supplementary Table 2. Relative gene expression was expressed in arbitrary units (A.U.) as a ratio of target transcripts normalized to murine cyclophilin or GAPDH mRNA level.

2.10. Immunofluorescence microscopy for intestinal GLUT2

Jejunal paraffin-embedded sections of five-micrometer thickness were unmasked in citrate buffer pH 6.0 for 10 min at 97 °C and incubated with primary antibody raised against GLUT2 (custom made, targeting the COOH-terminal; 1:500). Incubation with secondary antibodies (Cy3-conjugated donkey anti-rabbit: 1:1000; DAPI 1:1000 for nuclei staining) was performed. Localization of GLUT2 was examined using confocal microscopy (LSM710, Zeiss; 633 oil lens, 0.8 mm depth of field).

2.11. Immunohistochemistry for intestinal GLP-1

Jejunal and colon sections were treated as previously described [14]. Revelation was performed using the biotinylated secondary antibody/streptavidin-HRP amplification system (BIOSPA) and AEC (Vector laboratories, Inc). Sections were mounted in Glycergel Mounting Medium (Dako). Images were obtained using slide scanner (Axio Scan Z1, Zeiss). Measurement intestinal tissue area was performed using NIH Image J software.

2.12. Electron microscopy

Jejunum (morphological analyses) or colon (immunoelectron microscopy for intestinal GLP-1) samples were fixed with glutaraldehyde and paraformaldehyde after dissection. Jejunal ultra-thin sections (65 nm) were postfixed in osmic acid, then dehydrated in graded alcohol, embedded in Epon resin (Polysciences Inc), and counterstained with uranyl acetate and lead citrate using an LKB 2168 ultrastainer. After alcohol-graded dehydration, colon ultra-thin sections were embedded in polyhydroxy-aromatic acrylic LR-White resin and incubated with anti-GLP-1 antibody (Peninsula) followed by 12 nm gold particle-donkey anti-rabbit IgGs (Jackson ImmunoResearch Laboratories, Newmarket). For both stainings, sections were analyzed using Philips EM10 electron microscope coupled with an Erlangshen 1000 camera and software (Gatan; Roper Scientific). Measurement of microvillus length and quantifications of secretory granules and GLP-1 gold beads were performed with NIH Image J software.

2.13. Intestinal GLP-1 protein content

Proximal jejunum, distal ileum, and the whole colon were sliced into small pieces. Tissues were homogenized in ethanol/acid (100% ethanol: sterile water: 12N HCl 74:25:1 v/v) solution (5 mL/g tissue) and incubated overnight at 4 °C. The homogenates were centrifuged and supernatants were collected for total GLP-1 content measurement using ELISA method (GLP-1 Total ELISA kit, Millipore).

2.14. Statistical analysis

Results are expressed as mean $\pm$ SEM and median (range) for microbiota results, and the significance between the mean of continuous parameters was evaluated by 2-way ANOVA followed by Bonferroni post-test multiple comparisons or Mann−Whitney U test using PRISM software. All probabilities were two-tailed with significance set at $P < 0,05$.

3. RESULTS

3.1. Inducible invalidation of GLUT2 in mouse intestine

To induce GLUT2 invalidation specifically in the intestine, we administrated by gavage tamoxifen in *Slc2a2* $^{FLOX/FLOX} \times$ *Villin-CreERT2* $^{+/-}$ and *Slc2a2* $^{FLOX/FLOX} \times$ *Villin-CreERT2* $^{-/-}$ mice. We measured GLUT2 mRNA expression in the intestine and liver, another GLUT2 expressing tissue, up to 12 weeks post-invalidation. As expected, 4 weeks after tamoxifen administration, *Slc2a2* mRNA expression was markedly suppressed in the jejunum, ileum, and colon of GLUT2$^{\Delta IEC}$ mice as compared to control littermates without any change in the liver (Figure 1B). *Slc2a2* mRNA expression remained low in the intestine and unchanged in the liver even 12 weeks after tamoxifen administration (Figure 1B). *Slc2a2* mRNA loss led to an absence of GLUT2 protein at the membrane of jejunal epithelial cells in GLUT2$^{\Delta IEC}$ mice (Figure 1C).

3.2. Metabolic phenotype

3.2.1. Intestinal GLUT2 invalidation reduces glucose absorption

We first questioned the contribution of GLUT2 to intestinal glucose absorption in GLUT2$^{\Delta IEC}$ mice. *In vivo*, intestinal glucose absorption can be evaluated by the slope of increase in glycemia between 0 and 5 min after glucose gavage, which reflects the rate of glucose appearance in the bloodstream. Glycemic slopes were significantly decreased in GLUT2$^{\Delta IEC}$ throughout the 12-week invalidation period (Figure 2A), indicating glucose malabsorption in GLUT2$^{\Delta IEC}$ as compared to control mice.

Glucose malabsorption was still observed 12 weeks after tamoxifen administration but to a lesser extent, suggesting that compensatory mechanisms occurred (Figure 2A) such as overexpression of other sugar transporters. The expression of glucose transporters SGLT1,

administration (two-way ANOVA followed by Bonferroni correction for multiple comparisons). (**B**) Relative mRNA levels of sugar transporters SGLT1, GLUT1, GLUT3, GLUT5, and GLUT7 in the jejunum of control (white bars, n = 9−14) and GLUT2$^{\Delta IEC}$ (black bars, n = 7−13) mice, 4 (right panel) and 12 weeks (left panel) after tamoxifen administration. Values are means $\pm$ SEM. *P < 0.05; Control *vs* GLUT2$^{\Delta IEC}$ mice (Mann−Whitney U test). (**C**) Representative transversal, coronal, and sagittal PET-CT images of 2FDG accumulation in liver, kidney, bladder, stomach, intestine, heart, and brain of control (right panel) and GLUT2$^{\Delta IEC}$ (left panel) mice, 30 min after gavage of the tracer. (**D−H**) 60-min tracer activity detected in major target organs and tissues including kidney (D), bladder (E), liver (F), brain (G), and stomach (H) in control (white circles, n = 7) and GLUT2$^{\Delta IEC}$ mice (black circles, n = 9), 4 weeks after tamoxifen administration. Values are expressed as mean tissue radioactive concentration normalized by total orally administered 2FDG and body weight $\pm$ SEM (SUV: standardized uptake values). (**I**) Intestinal transit time. First appearance of dye in the feces after carmine red gavage given to control (white bar, n = 6) and GLUT2$^{\Delta IEC}$ mice (black bar, n = 5) after 6 h of fasting. Values are means $\pm$ SEM. ns: non-significant. (**J**) Representative PET-CT images of 2FDG accumulation in *ex vivo* flushed small intestine of control (right panel) and GLUT2$^{\Delta IEC}$ (left panel) mice, 60 min after gavage of the tracer. Delineation of small intestine with dotted lines. (**K**) *Ex vivo* tissue profiling for glucose tracer contents along the flushed small intestine of control (white circles, n = 6) and GLUT2$^{\Delta IEC}$ (black circles, n = 6) mice, 60 min after an intragastric glucose bolus (4 g/kg) containing 2FDG. Values are means $\pm$ SEM. *P < 0.05; control *vs* GLUT2$^{\Delta IEC}$ mice (two-way ANOVA).

GLUT1, GLUT3, and GLUT7 remained unchanged in the jejunum 4 and 12 weeks after tamoxifen administration in GLUT2$^{\Delta IEC}$ mice (Figure 2B). Interestingly, the expression level of fructose transporter GLUT5 was significantly increased 12 weeks after tamoxifen administration, supporting a compensatory mechanism for fructose absorption in GLUT2$^{\Delta IEC}$ mice (Figure 2B).

3.2.2. Short-term distribution of oral sugar (2FDG) is delayed in tissues of GLUT2$^{\Delta IEC}$ mice

To investigate the consequences of glucose malabsorption, we evaluated sugar distribution in tissues of GLUT2$^{\Delta IEC}$ mice. We gave orally 2FDG in a highly concentrated glucose bolus and recorded 2FDG biodistribution by PET imaging (Figure 2C). 2FDG biodistribution curves
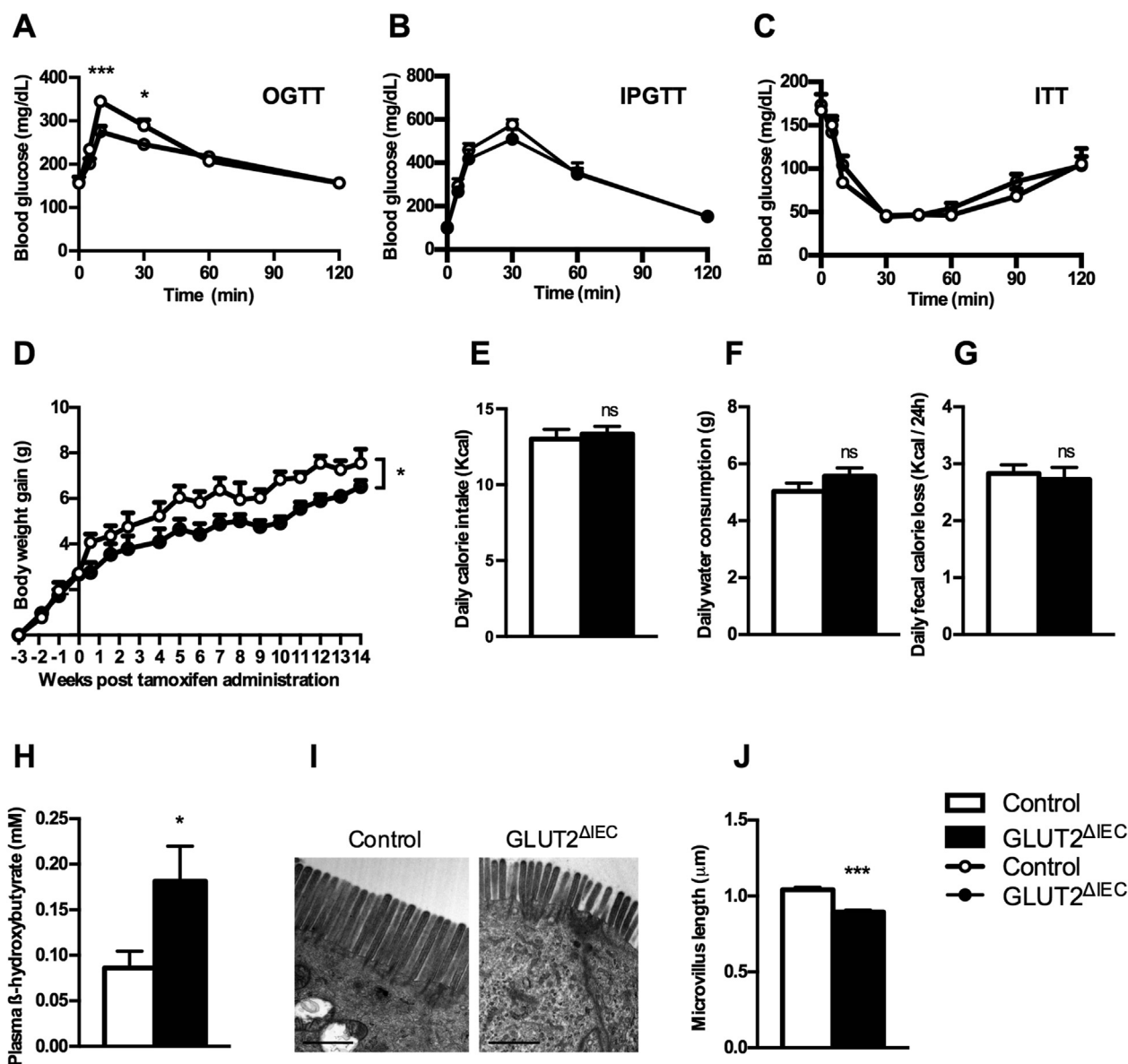

Figure 3: Intestinal GLUT2 invalidation improves mouse metabolism. (**A**) Oral glucose tolerance test (4 g glucose/kg) was performed in control (white circles, n = 16) and GLUT2$^{\Delta IEC}$ mice (black circles, n = 13) after 16 h of fasting, 4 weeks after tamoxifen administration. Values are means ± SEM; *P < 0.05; ***P < 0.001; control vs GLUT2$^{\Delta IEC}$ mice (two-way ANOVA followed by Bonferroni correction for multiple comparisons). (**B**) Intraperitoneal glucose tolerance test (4 g glucose/kg) was performed in control (white circles, n = 6) and GLUT2$^{\Delta IEC}$ mice (black circles, n = 10) after 16 h of fasting, 4 weeks after tamoxifen administration. Values are means ± SEM. (**C**) Insulin tolerance test (1 U insulin/kg) was performed in control (white circles, n = 9) and GLUT2$^{\Delta IEC}$ mice (black circles, n = 8) after 6 h of fasting, 4 weeks after tamoxifen administration. Values are means ± SEM. (**D**) Body weight gain follow-up 14 weeks after tamoxifen administration in control mice (white circles, n = 5) and GLUT2$^{\Delta IEC}$ mice (black circles, n = 6). Values are means ± SEM. *P < 0.05; control vs GLUT2$^{\Delta IEC}$ mice (Two-way ANOVA). (**E, F**) Daily calorie intake (B) and daily water consumption (C) measured in metabolic cages in control (white bars, n = 5) and GLUT2$^{\Delta IEC}$ mice (black bars, n = 6), 4 weeks after tamoxifen administration. Values are means ± SEM. ns: non-significant. (**G**) Loss of fecal calories was determined by bomb calorimetry analyses in 24 h feces collected from control (white bar, n = 10) and GLUT2$^{\Delta IEC}$ mice (black bar, n = 11), 4 weeks after tamoxifen administration. Values are means ± SEM. ns: non-significant. (**H**) Plasma levels of β-hydroxybutyrate were measured in fed control (white bars, n = 11) and GLUT2$^{\Delta IEC}$ mice (black bars, n = 15), 4 weeks after tamoxifen administration. Values are means ± SEM. *P < 0.05; control vs GLUT2$^{\Delta IEC}$ mice (Mann−Whitney U test). (**I**) Representative images of brush border electron microscopy from the jejunum of control (left panel) and GLUT2$^{\Delta IEC}$ mice (right panel), 4 weeks after tamoxifen administration. Scale bar = 1 μm. (**J**) Measurement of microvillus length from electron microscopy microphotographs of control (white bar) and GLUT2$^{\Delta IEC}$ mice (black bar), 4 weeks after tamoxifen administration. 230−250 microvilli were measured for each genotype. Values are means ± SEM. ***P < 0.001; Control vs GLUT2$^{\Delta IEC}$ mice (Mann−Whitney U test).
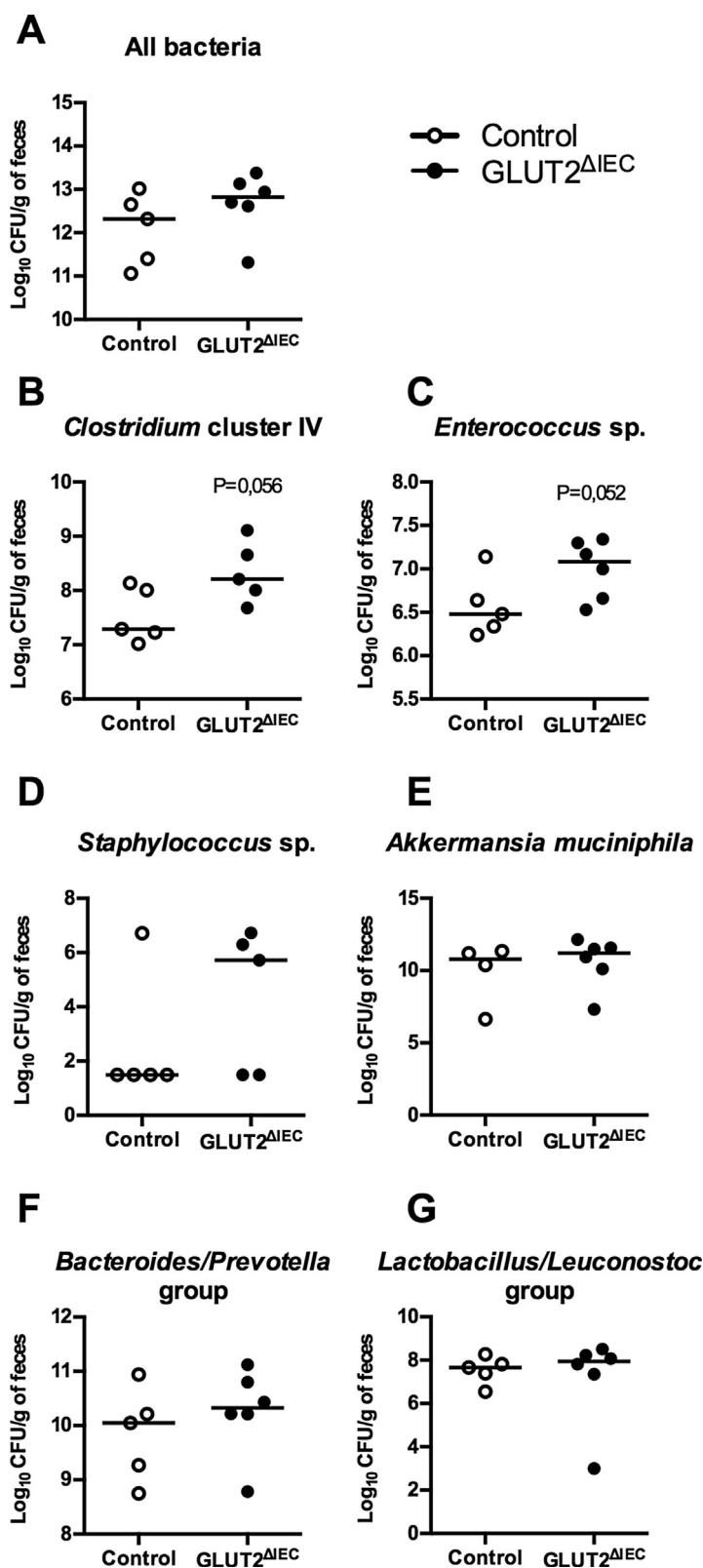
Figure 4: Intestinal GLUT2 invalidation changes fecal microbiota composition. (**A**) Total fecal bacterial counts in control (white circles, n = 5) and GLUT2$^{\Delta IEC}$ mice (black circles, n = 6), 4 weeks after tamoxifen administration. Values are median (range). (**B**−**G**) Fecal quantification of *Clostridium* cluster IV (**B**), *Enterococcus* sp. (**C**), *Staphylococcus* sp. (**D**), *Akkermansia muciniphila* (**E**), *Bacteroides/Prevotella* group (**F**) and *Lactobacillus/Leuconostoc* group (**G**) in control (white circles, n = 4−5) and GLUT2$^{\Delta IEC}$ mice (black circles, n = 5−6), 4 weeks after tamoxifen administration. Values are medians (range). P values are presented according to the Mann−Whitney *U* test.

from kidney (Figure 2D), bladder (Figure 2E), liver (Figure 2F), brain (Figure 2G), and stomach (Figure 2H) enabled the calculation of 2FDG accumulation slopes every 5 min over the first 30-min period. These measurements highlighted that 2FDG appeared more slowly in bladder (P = 0.0444) and in kidney (P = 0.139) of GLUT2$^{\Delta IEC}$ compared to control mice. Slopes of 2FDG appearance in bladder can be considered as an index of 2FDG apparition in the bloodstream due to the lack of 2FDG reabsorption by the kidneys. Furthermore, we also observed a 2FDG accumulation delay in liver (P = 0.0507) in GLUT2$^{\Delta IEC}$ compared to control mice. Indeed, we calculated a 10-min delay to achieve 50% of maximal 2FDG incorporation in liver in GLUT2$^{\Delta IEC}$ compared to control mice (Figure 2F). Interestingly, we could not observe any difference in the brain between the 2 groups of mice (P = 0.2616), suggesting a preferential glucose biodistribution to the brain compared to other tissues.

Differences in 2FDG biodistribution could be a consequence of delayed intestinal glucose absorption, which could not be attributed to a defect in gastric emptying (Figure 2H) or intestinal transit duration (Figure 2I). *Ex vivo* examination of flushed intestine showed a significant reduction of 2FDG accumulation the first half small intestinal mucosa of GLUT2$^{\Delta IEC}$ compared to control mice (P = 0.0187) (Figure 2J,K). This corresponds to the duodenum, jejunum, and very proximal ileum, where GLUT2 is mostly expressed in control mice. This experiment was performed with a high dose of glucose (10 MBq 2FDG in a saline solution containing 4 g/kg of D-glucose), which results in apical GLUT2 recruitment. Moreover, 2FDG is poorly transported through SGLT1. Therefore, 2FDG enters through GLUT2 in enterocytes of control mice, which could not occur in GLUT2$^{\Delta IEC}$ mice.

Thus, we propose that sugar absorption and distribution were delayed and moderately decreased by intestinal GLUT2 invalidation in mice.

3.2.3. Intestinal GLUT2 invalidation improves glucose tolerance and limits body weight gain

To investigate the consequences of intestinal GLUT2 invalidation on glucose homeostasis, we evaluated glucose tolerance and insulin sensitivity. GLUT2$^{\Delta IEC}$ mice display significantly improved oral glucose tolerance compared to control littermates (Figure 3A). However, intraperitoneal glucose tolerance was similar in both groups (Figure 3B). Improved oral glucose tolerance was independent of insulin sensitivity, which did not differ between groups (Figure 3C).

Intestinal GLUT2 invalidation caused a decrease in body weight gain in GLUT2$^{\Delta IEC}$ compared to control littermates throughout the 14 weeks of experiment (P = 0.0486) (Figure 3D). This occurred despite similar food intake (Figure 3E), water intake (Figure 3F), and total fecal calorie loss (Figure 3G) in both groups. Decreased body weight gain, therefore, could be attributed to glucose malabsorption.

Metabolite plasma measurements showed a significantly higher level of β-hydroxybutyrate in GLUT2$^{\Delta IEC}$ compared to control mice (Figure 3H, P = 0.0433) with no change in other plasma metabolites measured (data not shown). Ketone body production such as β-hydroxybutyrate in GLUT2$^{\Delta IEC}$ mice is reminiscent of fasting state or caloric restriction.

3.3. Gut phenotype

3.3.1. Absorption surface is reduced in the intestine of GLUT2$^{\Delta IEC}$ mice

Importantly, we observed a significant decrease (P < 0,001) of microvillus length in the jejunum of GLUT2$^{\Delta IEC}$ as compared to control mice (Figure 3I and J), mimicking a condition of food deprivation. This

15% diminution in microvillus length reduces the absorbing epithelial surface and, thus, could further limit the absorption of nutrients.

3.3.2. Intestinal GLUT2 invalidation changes microbiota composition

The signs of glucose malabsorption described in GLUT2$^{\Delta IEC}$ mice suggest glucose persistence in the intestinal lumen that might affect gut bacterial composition. Despite similar total bacteria counts (Figure 4A), *Clostridium* cluster IV (Figure 4B, P = 0.056) and *Enterococcus* sp. (Figure 4C, P = 0.052), levels were increased in fecal microbiota from GLUT2$^{\Delta IEC}$ compared to control mice. Concerning *Staphylococcus* sp. (Figure 4D), two populations appeared in each group: mice are either not colonized or colonized at high level with *Staphylococci*. Other studied species (i.e. *Akkermansia muciniphila*), or groups (i.e. *Bacteroidetes/Prevotella* and *Lactobacillus/Leuconostoc*) remained unaffected (Figure 4E−G).

3.3.3. Intestinal GLUT2 invalidation decreases gut permeability and improves gut inflammatory status

Because modulation of gut microbiota is often associated with modification in gut barrier function, we investigated the impact of intestinal
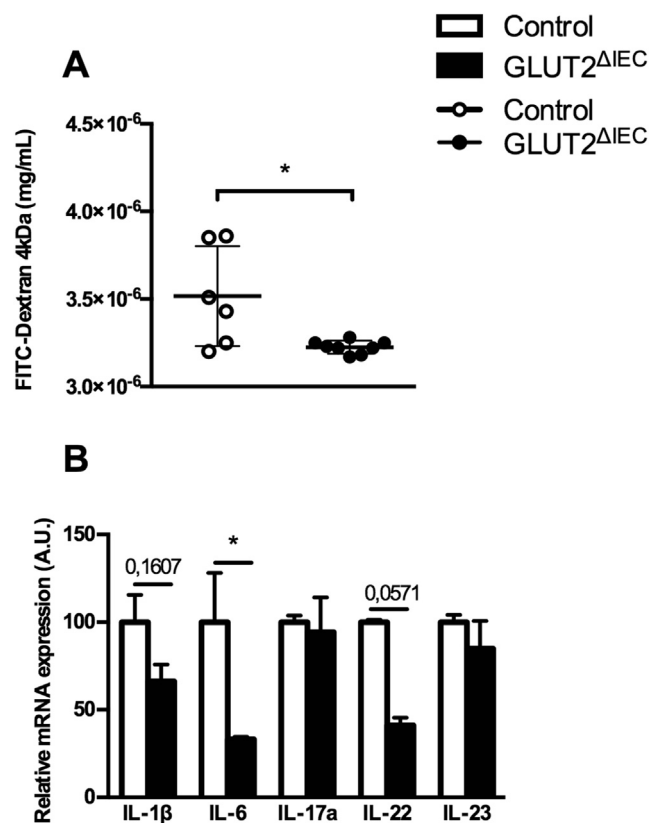

Figure 5: Intestinal GLUT2 invalidation reduces jejunal permeability and inflammatory status. (**A**) Jejunum permeability was measured in control mice (white circles, n = 6) and GLUT2$^{\Delta IEC}$ mice (black circles, n = 8) by Ussing Chamber method. FD4 concentration was measured in serosal compartment after a 180-min period. Values are means ± SEM. *P < 0.05; control *vs* GLUT2$^{\Delta IEC}$ mice (Mann−Whitney *U* test). (**B**) Relative mRNA levels of pro-inflammatory cytokines IL-1β, IL-6, IL-17, IL-22 and IL-23 in ileal *lamina propria* lymphocytes of control (white bars, n = 4−5) and GLUT2$^{\Delta IEC}$ mice (black bars, n = 3), 4 weeks after tamoxifen administration. Values are means ± SEM. *P < 0.05; Control *vs* GLUT2$^{\Delta IEC}$ mice (Mann−Whitney *U* test).

GLUT2 invalidation on permeability using Ussing Chamber method (Figure 5A). Interestingly, there was a significantly decreased permeability in the jejunum of GLUT2$^{\Delta IEC}$ compared to control mice. Permeability is also affected by inflammatory signals and we high-lighted here a decrease of mRNA coding for pro-inflammatory cyto-kines IL-6 (P = 0.0357) and IL-22 (P = 0.0571) but no change for the expression of IL-1β (P = 0.1607), IL-17a (P = 0.8571) or IL-23 (P = 0.2143) in the ileum of GLUT2$^{\Delta IEC}$ mice compared to that of control mice (Figure 5B). The gut inflammatory status of GLUT2$^{\Delta IEC}$ mice was thus slightly decreased after the invalidation of intestinal GLUT2 suggesting that sugar availability is coupled with permeability and inflammation in gut.

3.3.4. Intestinal GLUT2 invalidation reduces density but improves function of GLP-1 positive cells

As GLUT2 is also expressed in GLP-1 positive cells, we investigated L-cell homeostasis in GLUT2$^{\Delta IEC}$ mice. We first measured the density of GLP-1 positive cells (L-cells) in the intestine of GLUT2$^{\Delta IEC}$ and control mice (Figure 6A and B). Surprisingly, there was a significant decrease of L-cell density in jejunum (50%, P = 0.0053) and a tendency to lower density in colon (20% reduction, P = 0.147) of GLUT2$^{\Delta IEC}$ as compared to control mice (Figure 6B). Despite this lower L-cell density in GLUT2$^{\Delta IEC}$ mice, both intestinal total GLP-1 content (Figure 6C) and plasma active GLP-1 concentration (Figure 6D) remained unaltered when compared to control mice. The preservation of enteroendocrine
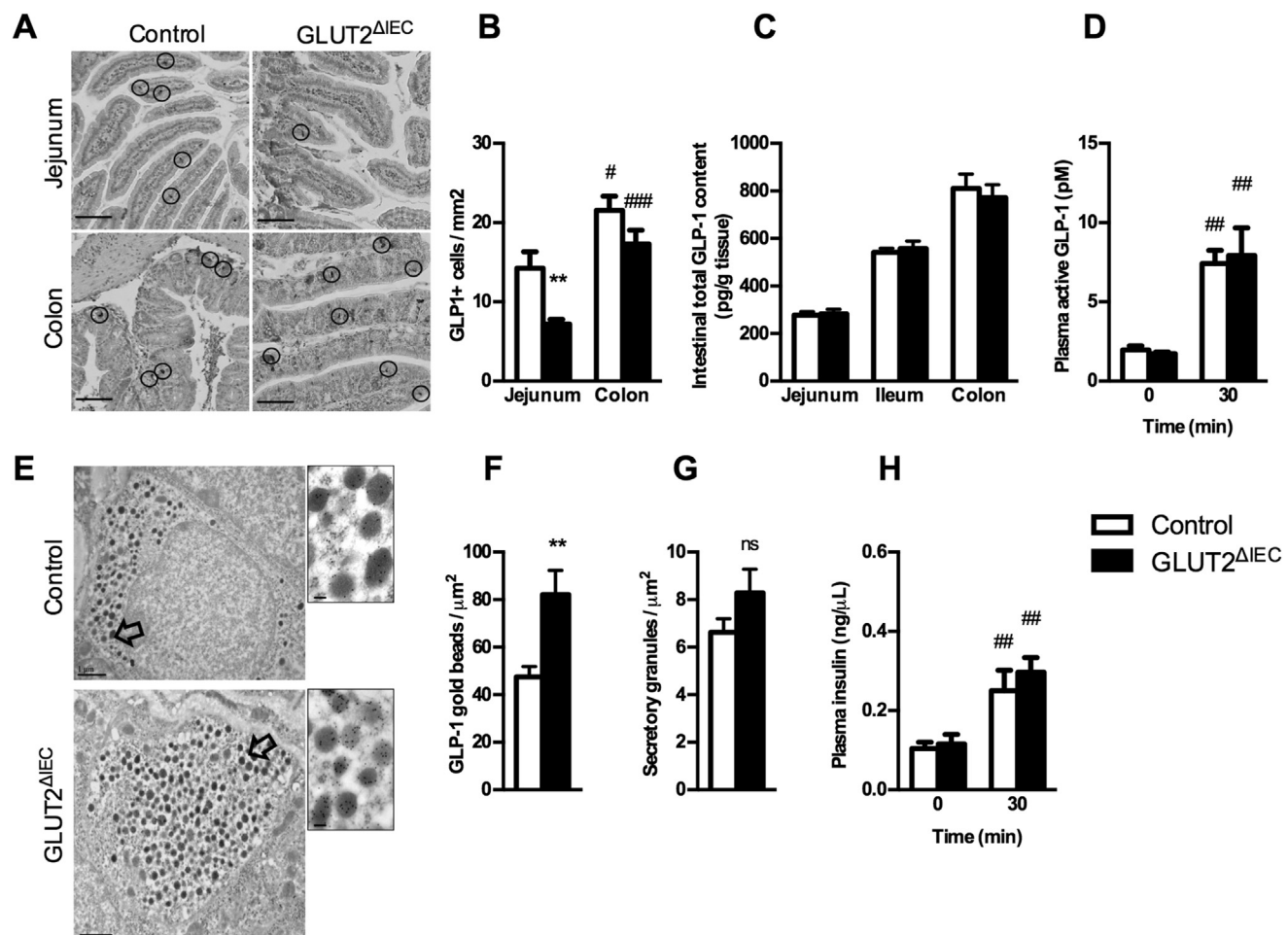

Figure 6: Intestinal GLUT2 invalidation reduces GLP-1-producing cell density in the jejunum. (A) Representative images of GLP-1 immunostaining in jejunum and colon sections from control (left panel) and GLUT2$^{\Delta IEC}$ mice (right panel), 4 weeks after tamoxifen administration. GLP-1 immunoreactive cells are circled. Scale bar = 100 μm. (B) Number of GLP-1 immunoreactive cells per mm^2 in the jejunum and colon of control (white bars, n = 15) and GLUT2$^{\Delta IEC}$ mice (black bars, n = 11), 4 weeks after tamoxifen administration. Values are means ± SEM. **P < 0.01; control vs GLUT2$^{\Delta IEC}$ mice. #P < 0.05; ###P < 0.001 jejunum *vs* colon (Mann−Whitney *U* tests). (C) Intestinal total GLP-1 contents (pmol/g of tissue) were measured in jejunum, ileum, and colon samples of control (white bars, n = 9) and GLUT2$^{\Delta IEC}$ mice (black bars, n = 9), 4 weeks after tamoxifen administration. Values are means ± SEM. (D) Plasma active GLP-1 concentrations after a bolus of 2 g glucose/kg + 200 μL olive oil were measured in control (white bars, n = 10) and GLUT2$^{\Delta IEC}$ mice (black bars, n = 11), 4 weeks after tamoxifen administration. Values are means ± SEM. ##P < 0.01; 0 *vs* 30 min (Mann−Whitney *U* test). (E) Representative electron microscopy images of enteroendocrine L-cells labeled with anti-GLP-1-coupled immunogold beads from colon of control (top panel) and GLUT2$^{\Delta IEC}$ mice (bottom panel). Scale bar: 1 μm (entire image) and 100 nm (magnification). (F) Number of anti-GLP-1-coupled immunogold beads (included in a secretory granule) per μm^2 in the colon of control (white bar, 29 L-cells) and GLUT2$^{\Delta IEC}$ mice (black bar, 14 L-cells), 4 weeks after tamoxifen administration. Values are means ± SEM. **P < 0.01; control *vs* GLUT2$^{\Delta IEC}$ mice (Mann−Whitney *U* test). (G) Number of secretory granules per μm^2 in the colon of control (white bar, 30 L-cells) and GLUT2$^{\Delta IEC}$ mice (black bar, 14 L-cells), 4 weeks after tamoxifen administration. Values are means ± SEM. ns: non-significant. (H) Basal and stimulated plasma insulin concentrations after an oral challenge of 2 g glucose/kg + 200 μL olive oil assessed in control (white bars, n = 10) and GLUT2$^{\Delta IEC}$ mice (black bars, n = 11), 4 weeks after tamoxifen administration. Values are means ± SEM. ##P < 0.01; 0 *vs* 30 min (Mann−Whitney *U* test).

function could be explained by an 80% higher GLP-1 content per L-cell in GLUT2$^{\Delta IEC}$ mice as compared to control mice (Figure 6E and F). However, secretory granule density per L-cell was similar in the 2 groups of mice (Figure 6G) demonstrating a higher GLP-1 content per granule in GLUT2$^{\Delta IEC}$ mice. These data suggested that the residual L-cells present in the epithelium produce more GLP-1 to fulfill GLP-1 secretion in GLUT2$^{\Delta IEC}$ mice. Plasma GLP-1 was preserved in GLUT2$^{\Delta IEC}$ mice leading to a conserved plasma insulin concentration in GLUT2$^{\Delta IEC}$ mice as compared to control mice (Figure 6H).

4. DISCUSSION

We showed that intestinal GLUT2 invalidation provokes glucose malabsorption that delayed glucose biodistribution to tissues. The consequences of intestinal-specific invalidation of GLUT2 on mouse phenotype were limited weight gain and improved glucose tolerance and gut barrier function, which was associated with reduced gut inflammation. All these features have been reported in calorie restriction conditions [15]. Moreover, we showed that gut epithelium homeostasis was challenged by sugar malabsorption. Indeed, microvillus length was reduced, and the change in microbiota composition, possibly related to persistence of malabsorbed glucose in the lumen of the distal intestinal segment, favored *Clostridium* cluster IV, a commensal *Clostridium* known to display protective roles on gut homeostasis. In addition, L-cell density was reduced in the absence of intestinal GLUT2 expression, but the GLP-1 content per L-cell was increased, suggesting preserved enteroendocrine L-cell function. Therefore, we propose that blocking intestinal GLUT2 function is a possible strategy to temper sugar biodistribution and, surprisingly, modulate gut epithelial homeostasis.

GLUT5 mRNA was doubled in the jejunum 12 weeks after tamoxifen administration, supporting a compensatory mechanism for fructose absorption in GLUT2$^{\Delta IEC}$ mice as previously suggested in Glut2$^{-/-}$; RIPGlut1 mice [2]. However, we could not observe any compensatory mechanism concerning intestinal glucose transport by overexpression of other glucose transporters. This could be explained by the existence of vesicular glucose transport that occurs in absence of GLUT2 as shown in Glut2$^{-/-}$; RIPGlut1 mice [10]. However, this mechanism is not sufficient to fully compensate for the absence of GLUT2 leading to moderate glucose malabsorption and reduced body weight gain in GLUT2$^{\Delta IEC}$ mice.

Invalidating mutations of GLUT2 are reported in patients [16]. Only double heterozygous or homozygous mutations in the *SLC2A2* gene-encoding GLUT2 (http://omim.org/entry/227810) have been found in infants with Fanconi—Bickel syndrome. These patients suffer from failure to thrive, glucose-galactose malabsorption, gross urinary loss of glucose, glycogen accumulation in liver and kidney, and, in some patients, diabetes. To restore patient growth, a ketogenic diet is proposed to Fanconi—Bickel patients. It has been reported that intestinal regulatory function of GLUT2 could be compensated by a ketogenic diet (frequent boluses of slowly absorbed carbohydrates, such as uncooked cornstarch). Caloric restriction without malnutrition is indeed characterized by ketosis and a slow-down of biological processes such as body weight gain, glucose metabolism [15], and gut inflammation [17—19] as well as decreased microvillus length [20]. Here, the doubling of plasma ketone body β-hydroxybutyrate in
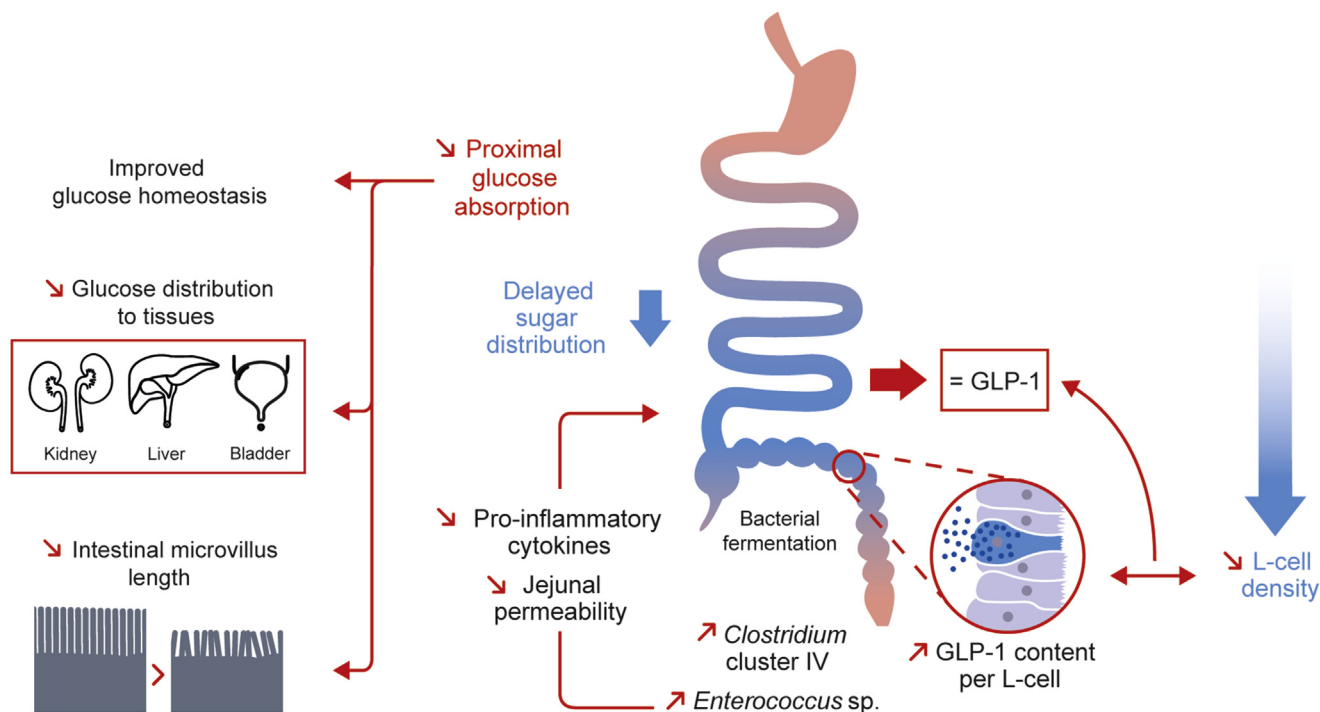

Figure 7: Intestinal GLUT2 plays a role in glucose and gut homeostasis in mice. Intestinal invalidation of GLUT2 in mice reduces proximal intestinal absorption of glucose. This sugar malabsorption modifies body homeostasis by means of 1) improving glucose homeostasis, 2) delaying tissue distribution of glucose to peripheral tissues, and 3) reducing intestinal microvillus length, which could result in a global nutrient malabsorption, mimicking caloric restriction. Our hypothesis is that blocked proximal glucose absorption causes an increased glucose delivery to distal intestine, giving new fermentable energy sources to the distal gut microbiota. Thus, we observed increased levels of commensal *Clostridium* cluster IV and *Enterococcus* sp. in our model. These bacteria show positive impact on gut homeostasis, including a reduced expression of pro-inflammatory cytokines through butyrate production and reduced gut permeability. Surprisingly, intestinal GLUT2 invalidation leads to a strong loss in enteroendocrine L-cell density, with no impact on GLP-1 plasma levels thanks to increased GLP-1 content per GLUT2$^{\Delta IEC}$ L-cell.

GLUT2^{ΔIEC} mice as a sign of a glucose restriction for tissue, could be attributed to delayed glucose delivery to tissues due to intestinal GLUT2 depletion.

GLUT2^{ΔIEC} mice displayed a reduction of both microvillus length and inflammation. This could be due to changes in microbiota composition caused by disturbed glucose abundance in the lumen. Indeed, *Clostridium* cluster IV, belonging to the Firmicutes phylum, is increased in GLUT2^{ΔIEC} mice. These commensal bacteria show a positive impact on gut homeostasis [21], including a reduced expression of pro-inflammatory cytokines through butyrate production [22,23]. *Enterococci* are also increased. Some members of this genus show anti-inflammatory properties, suggesting that this increase also can be associated with a suitable gut homeostasis. On the other hand, enteroendocrine cells are one of the cell types for which density in the gut epithelium is dependent on nutritional factors [14]. In our model, endocrine L-cell homeostasis was modulated by intestinal GLUT2 invalidation. Despite reduced L-cell density, enteroendocrine function seemed to be preserved through higher intracellular GLP-1 content. Recent papers showed that during OGTT in various types of metabolic diseases, GLP-1 release is delayed along with prolongation of the postprandial hyperglycaemia [24—26]. In our study, GLP-1 secretion was measured belatedly, 30 min after GLP-1 secretagogue administration. Therefore, we cannot exclude that the lack of intestinal GLUT2 is retarding glucose-induced GLP-1 release from the jejunum and therefore has consequences on glucose and gut homeostasis. The use of various metabolic stimuli and the measurement of plasma GLP-1 at earlier time points in GLUT2^{ΔIEC} to challenge L-cell function would be informative for enteroendocrine function.

5. CONCLUSION

Intestinal GLUT2 is known as a means to transfer glucose and fructose from the lumen to the bloodstream and, thereby, to provide sugar to tissue. Here, we extended the role of intestinal GLUT2 in sugar distribution to tissues and glucose homeostasis. In addition, invalidation of GLUT2 also revealed unexpected function for GLUT2 in regulating gut homeostasis such as modulating enteroendocrine L-cell density, microvillus length, gut permeability, and inflammation (Figure 7). Therefore, specifically blocking intestinal GLUT2 activity by the mean of drugs could be a strategy to protect against weight gain and metabolic perturbations.

AUTHORS' CONTRIBUTIONS

C.C.S., A.G. and P.S. designed experiments, acquired, analyzed data, and wrote the manuscript. T.A., T.V., A.J.W., C.M., O.R., and N.K. acquired data and contributed to the discussion. D.C. acquired and analyzed data. E.B.L. and M.L.G. generated GLUT2^{ΔIEC} and contributed to the discussion. A.Let. contributed to the discussion and wrote the manuscript. G.G., A.Leh., and B.T. contributed to the discussion.

PRIOR PRESENTATION

Part of these data were presented at 51st Annual Meeting of the European Association for the Study of Diabetes 2015 [27].

CONFLICT OF INTEREST

The authors declare no competing financial interests.

APPENDIX A. SUPPLEMENTARY DATA

Supplementary data related to this article can be found at http://dx.doi.org/10.1016/j.molmet.2016.10.008.

REFERENCES

[1] Thorens, B., 2015. GLUT2, glucose sensing and glucose homeostasis. Diabetologia 58(2):221—232. http://dx.doi.org/10.1007/s00125-014-3451-1.

[2] Gouyon, F., Caillaud, L., Carriere, V., Klein, C., Dalet, V., Citadelle, D., et al., 2003. Simple-sugar meals target GLUT2 at enterocyte apical membranes to improve sugar absorption: a study in GLUT2-null mice. The Journal of Physiology 552(Pt 3):823—832. http://dx.doi.org/10.1113/jphysiol.2003.049247.

[3] Kellett, G.L., Helliwell, P.A., 2000. The diffusive component of intestinal glucose absorption is mediated by the glucose-induced recruitment of GLUT2 to the brush-border membrane. The Biochemical Journal 350(Pt 1):155—162.

[4] Ait-Omar, A., Monteiro-Sepulveda, M., Poitou, C., Le Gall, M., Cotillard, A., Gilet, J., et al., 2011. GLUT2 accumulation in enterocyte apical and intracellular membranes: a study in morbidly obese human subjects and ob/ob and high fat-fed mice. Diabetes 60(10):2598—2607. http://dx.doi.org/10.2337/db10-1740.

[5] Reimann, F., Habib, A.M., Tolhurst, G., Parker, H.E., Rogers, G.J., Gribble, F.M., 2008. Glucose sensing in L cells: a primary cell study. Cell Metabolism 8(6):532—539. http://dx.doi.org/10.1016/j.cmet.2008.11.002.

[6] Helander, H.F., Fändriks, L., 2012. The enteroendocrine "letter cells" — time for a new nomenclature? Scandinavian Journal of Gastroenterology 47(1):3—12 http://dx.doi.org/10.3109/00365521.2011.638391.

[7] Kieffer, T.J., Habener, J.F., 1999. The glucagon-like peptides. Endocrine Reviews 20(6):876—913. http://dx.doi.org/10.1210/edrv.20.6.0385.

[8] Wang, Z., Wang, R.M., Owji, A.A., Smith, D.M., Ghatei, M.A., Bloom, S.R., 1995. Glucagon-like peptide-1 is a physiological incretin in rat. The Journal of Clinical Investigation 95(1):417—421. http://dx.doi.org/10.1172/JCl117671.

[9] Pais, R., Gribble, F.M., Reimann, F., 2016. Stimulation of incretin secreting cells. Therapeutic Advances in Endocrinology and Metabolism 7(1):24—42. http://dx.doi.org/10.1177/2042018815618177.

[10] Stümpel, F., Burcelin, R., Jungermann, K., Thorens, B., 2001. Normal kinetics of intestinal glucose absorption in the absence of GLUT2: evidence for a

transport pathway requiring glucose phosphorylation and transfer into the endoplasmic reticulum. Proceedings of the National Academy of Sciences of the United States of America 98(20):11330–11335. http://dx.doi.org/10.1073/pnas.211357698.

[11] Cani, P.D., Holst, J.J., Drucker, D.J., Delzenne, N.M., Thorens, B., Burcelin, R., et al., 2007. GLUT2 and the incretin receptors are involved in glucose-induced incretin secretion. Molecular and Cellular Endocrinology 276(1–2):18–23. http://dx.doi.org/10.1016/j.mce.2007.06.003.

[12] El Marjou, F., Janssen, K.-P., Chang, B.H.-J., Li, M., Hindie, V., Chan, L., et al., 2004. Tissue-specific and inducible Cre-mediated recombination in the gut epithelium. Genesis 39(3):186–193. http://dx.doi.org/10.1002/gene.20042 (New York, N.Y.: 2000).

[13] Neau, E., Delannoy, J., Marion, C., Cottart, C.-H., Labellie, C., Holowacz, S., et al., 2016. Three novel candidate probiotic strains with prophylactic properties in a murine model of Cow's milk allergy. Applied and Environmental Microbiology 82(6):1722–1733. http://dx.doi.org/10.1128/AEM.03440-15.

[14] Aranias, T., Grosfeld, A., Poitou, C., Omar, A.A., Le Gall, M., Miquel, S., et al., 2015. Lipid-rich diet enhances L-cell density in obese subjects and in mice through improved L-cell differentiation. Journal of Nutritional Science 4:e22. http://dx.doi.org/10.1017/jns.2015.11.

[15] Heilbronn, L.K., Ravussin, E., 2003. Calorie restriction and aging: review of the literature and implications for studies in humans. The American Journal of Clinical Nutrition 78(3):361–369.

[16] Santer, R., Steinmann, B., Schaub, J., 2002. Fanconi-Bickel syndrome—a congenital defect of facilitative glucose transport. Current Molecular Medicine 2(2):213–227.

[17] Meydani, S.N., Das, S.K., Pieper, C.F., Lewis, M.R., Klein, S., Dixit, V.D., et al., 2016. Long-term moderate calorie restriction inhibits inflammation without impairing cell-mediated immunity: a randomized controlled trial in non-obese humans. Aging 8(7):1416–1431. http://dx.doi.org/10.18632/aging.100994.

[18] Most, J., Tosti, V., Redman, L.M., Fontana, L., 2016. Calorie restriction in humans: an update. Ageing Research Reviews. http://dx.doi.org/10.1016/j.arr.2016.08.005.

[19] Ravindran, R., Loebbermann, J., Nakaya, H.I., Khan, N., Ma, H., Gama, L., et al., 2016. The amino acid sensor GCN2 controls gut inflammation by inhibiting inflammasome activation. Nature 531(7595):523–527. http://dx.doi.org/10.1038/nature17186.

[20] Wang, T., Hung, C.C.Y., Randall, D.J., 2006. The comparative physiology of food deprivation: from feast to famine. Annual Review of Physiology 68:223–251. http://dx.doi.org/10.1146/annurev.physiol.68.040104.105739.

[21] Lopetuso, L.R., Scaldaferri, F., Petito, V., Gasbarrini, A., 2013. Commensal Clostridia: leading players in the maintenance of gut homeostasis. Gut Pathogens 5(1):23. http://dx.doi.org/10.1186/1757-4749-5-23.

[22] Lührs, H., Gerke, T., Schauber, J., Dusel, G., Melcher, R., Scheppach, W., et al., 2001. Cytokine-activated degradation of inhibitory kappaB protein alpha is inhibited by the short-chain fatty acid butyrate. International Journal of Colorectal Disease 16(4):195–201.

[23] Segain, J.P., Raingeard de la Blétière, D., Bourreille, A., Leray, V., Gervois, N., Rosales, C., et al., 2000. Butyrate inhibits inflammatory responses through NFkappaB inhibition: implications for Crohn's disease. Gut 47(3):397–403.

[24] Junker, A.E., Gluud, L., Holst, J.J., Knop, F.K., Vilsbøll, T., 2016. Diabetic and nondiabetic patients with nonalcoholic fatty liver disease have an impaired incretin effect and fasting hyperglucagonaemia. Journal of Internal Medicine 279(5):485–493. http://dx.doi.org/10.1111/joim.12462.

[25] Dalla Man, C., Micheletto, F., Sathananthan, M., Vella, A., Cobelli, C., 2016. Model-based quantification of glucagon-like peptide-1-induced potentiation of insulin secretion in response to a mixed meal challenge. Diabetes Technology & Therapeutics 18(1):39–46. http://dx.doi.org/10.1089/dia.2015.0146.

[26] Nguyen, N.Q., Debreceni, T.L., Bambrick, J.E., Chia, B., Wishart, J., Deane, A.M., et al., 2015. Accelerated intestinal glucose absorption in morbidly obese humans: relationship to glucose transporters, incretin hormones, and glycemia. The Journal of Clinical Endocrinology and Metabolism 100(3):968–976. http://dx.doi.org/10.1210/jc.2014-3144.

[27] Schmitt, C., Aranias, T., Carriere, V., Ribeiro, A., Garbin, K., Le Gall, M., et al., 2015. Intestinal GLUT2 invalidation leads to glucose malabsorption and reduces enteroendocrine cell density. Diabetologia 58. S273–S273.